Photoinduced Structural Change in MgO Single Crystal

Taira Sakurai*, Yasuhiko Shimotsuma, Masahiro Shimizu, and Kiyotaka Miura

Department of Material Chemistry, Kyoto University, Japan
**Corresponding author's e-mail: sakurai.taira.55x@st.kyoto-u.ac.jp*

The photoexcited structural changes by the femtosecond laser pulses is one of the basic principles for laser processing techniques such as cutting and slicing. The femtosecond laser pulses photoexcite various structural changes of defects and nanovoids in MgO single crystals, and then such deficiencies develop into cracks. However, the precise roles of laser polarization during this process are unknown. Here we show that the photoinduced defects and nanovoids were formed along the <100> direction corresponding to the slip plane. Remarkably, the distribution of defects and nanovoids in [100] and [010] directions changed according to the polarization direction, resulting in polarization-dependent birefringence. Furthermore, depending on the pulse energy, the laser damage along the scanning direction was observed in the lower part of the focal region due to multiple filamentations.
DOI: 10.2961/jlmn.2024.01.2008
Keywords: femtosecond laser, MgO single crystal, birefringence, crystal structure, multiple filamentation

1. Introduction

In the past decade, the light source of femtosecond laser has rapidly spread in various fields, including communications [1,2], medicine [3,4], and measurement [5,6]. Particularly, in the field of laser processing, based on the various structural changes induced by the femtosecond laser into transparent materials, not only the precise material processing but also the fabrication of many optical devices such as optical waveguides [7,8], fiber Bragg gratings [5,9,10], optical storages [11,12], can be achieved. It is known that such structural changes are strongly influenced by the crystal structure. For example, it has been reported that nonlinear absorption due to the anisotropy of the effective mass of electrons depends on the crystal structure [13]. We have also observed that dislocations and cracks generate and propagate depending on the crystal structure due to the anisotropy of shock wave propagation [14-18]. More recently, we have also simulated the polarization dependence of electron dynamics after photoexcitation, by using the time-dependent density-functional theory (TDDFT) [19]. More interesting structural changes can be created by focusing the femtosecond laser pulses in materials. A polarization-dependent periodic nanostructure is successfully self-assembled in the center of the photoexcited region [20-25]. So far, such nanogratings have been observed in some glasses comprised mainly of a network-former oxide such as SiO_2 and GeO_2 [20,21], and in some crystals such as SiC and Si [23,24]. We found that the direction of the nanograting in a Si crystal is different from that in SiO_2 glass [24]. These differences could be derived from the polarization dependence of photoexcited electrons [26] and the electronic stress [27], but the details have not been clarified. Recently, we reported that color centers in fluoride single crystals of LiF, CaF_2, and BaF_2 are distributed in the direction perpendicular to the polarization direction after the femtosecond laser irradiation [25]. Such structure exhibits birefringence with a slow axis in the direction perpendicular to the polarization direction, which is similar to that of silica glass. In this study, we investigated the structural changes in a MgO single crystal. Unlike SiO_2 glass with no definite regular structure, in the center of the photoexcited region of MgO crystal, the formation direction of defects and nanovoids was limited to the <100> direction corresponding to the slip plane. The ratio of defects and nanovoids in [100] and [010] directions remarkably changed according to the polarization direction, resulting in polarization-dependent birefringence. Furthermore, depending on the pulse energy, the laser damage along the scanning direction was also observed in the lower part of the focal region due to multiple filamentations.

2. Experiments

In the experiments we used a mode-locked Ti: Sapphire laser (λ=800 nm, 1 kHz, 100 fs). The laser beam was focused 100 μm below the surface of a MgO single crystal in (100) plane with a 50× objective lens (NA = 0.80). The pulse energy was varied from 1 μJ to 40 μJ. Two kinds of laser irradiation methods with and without scanning of the focus were employed. The number of pulses was set to 1000 pulses in the experiment without scanning. In the experiment with scanning, the scanning speed of focus was set to 100 μm/s corresponding to 10 pulses for every 1 μm, assuming that the diameter of the photoexcited region is about 10 μm. The polarization direction was varied from 0° to 90° using a half-wave plate and was denoted as the angle from [100] axis, namely the polarization direction of 90° was parallel to the [010] axis. After laser irradiation, the focal region was inspected by an optical microscope and a polarized optical microscope. To analyze the detailed structure at the focal region, we polished and then etched the sample surface with 5 vol% phosphoric acid for 90 minutes at room temperature and observed the etched surface by a field emission scanning electron microscope (FE-SEM). We have also observed the microscopic structural changes by using a transmission electron microscope (TEM).

3. Fixed-point irradiation

We show the results of polarized optical microscope observation in Fig. 1. Two kinds of birefringence are observed from the polarized optical microscope images. One is cross-patterning birefringence in <110> directions around the focal region, and this is known to be derived from dislocations [14]. Another is polarization-dependent birefringence at the focal region. The retardance at the laser-processed region first increased linearly as the pulse energy was increased up to 10 μJ and after that, temporal saturation or slight decrease was observed. [Fig. 1(c)]. A spot which has no birefringence was observed at the center of the photoexcited region with 20 μJ or more pulse energies [Fig. 1(b)]. This indicates that the destructive breakdown with pulse energies above 20 μJ occurred at the center region. In the following experiments, therefore, the pulse energy was set to 20 μJ.

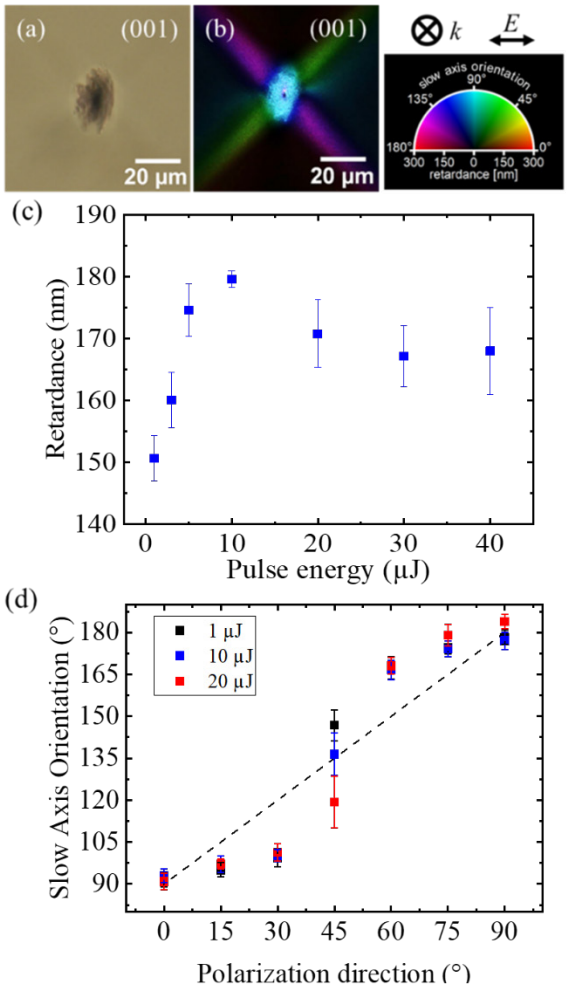

Fig. 1 Typical images of (a) optical microscope and (b) polarized optical microscope of the laser-processed region in MgO (001) plane. Symbols of *E* and *k* show the laser polarization and propagation direction, respectively. The laser parameters are 800 nm, 1 kHz, 100 fs, 20 μJ, and 1000 pulses, respectively. (c) Phase retardation of birefringence at the laser-processed region in MgO as a function of laser pulse energy. (d) Plots of the slow axis orientation versus the laser polarization direction. The dashed line shows an ideal slow axis orientation perpendicular to the laser polarization direction.

The slow axis orientation at the overall photoexcited region tends to be perpendicular to the femtosecond laser polarization direction [Fig.1(d)]. However, there was a large gap between the measured slow axis values and the ideal values in the polarization direction of 15° to 75°. To reveal the origin of the spot showing no birefringence and the gap in the slow axis orientation, we performed FE-SEM observation of the upper and lower part of the irradiated area by changing the polishing depth in steps [Fig. 2]. The lower part was located at about 30 μm deeper than the upper part.

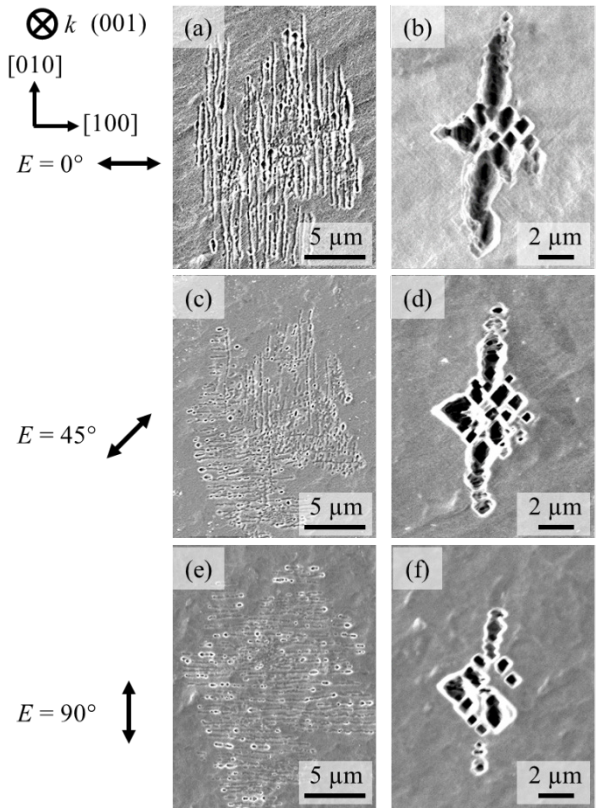

Fig. 2 SEIs of the upper part (a, c, e) and the lower part (b, d, f) of the laser processed region with the different polarization directions (*E*).

From the secondary electron images (SEIs) of the upper part, grooves with a width of about 100 nm were observed [Fig. 2(a, c, e)]. Some studies have revealed that oxygen defects are formed by beam irradiation of a neutron and an electron into a MgO single crystal [28,29]. Taking into account these results, we can identify that the grooves induced by laser irradiation consist of the array of oxygen defects and nanovoids, which are selectively etched. The formation of polarization-dependent nanograting composed of oxygen defects and nanovoids has first been observed in silica glass [20]. Up to now, such nanostructures exhibiting optical anisotropy have also been confirmed in several crystals [30-32]. The anisotropic distribution of the nanostructure with a lower refractive index exhibits a negative form-birefringence with an azimuth angle perpendicular to the laser polarization direction. The analogous situation seemingly applies to MgO single crystal. However, the structural change for MgO single crystal is unlike that for silica glass. Namely,

nanovoids in silica glass are always perpendicular to the polarization direction. In contrast, nanovoids in a crystal structure are distributed only in a certain direction corresponding to the slip plane. In the case of MgO crystal with a NaCl-type crystal structure, the slip planes are along the (100) and (010). If the polarization direction is 45°, specifically, the polarization vector of the electric field is equally divided along the (100) and (010). The formation of defects and nanovoids distributed in the direction along the {110} plane was hardly observed, while they were distributed in the <100> and <010> direction along the slip plane [Fig. 2(c)]. Furthermore, according to the proposed mechanisms of nanograting formation such as the interference between incident light and plasma waves [20] and the asymmetric growth of nanoplasmonics [33], the azimuth of the nanograting responds nonlinearly to the intensity of the electric field of light. For instance, in the case of the polarization direction of 60°, the ratio of the electric field components in [100] and [010] direction is $1:\sqrt{3}$. Considering that n-photons are involved in nanograting formation, the contribution of the electric field to the azimuth of birefringence in the [100] and [010] directions can be $3^{\frac{n}{2}}:1$. As a result, for polarization directions larger than 60° (or smaller than 30°), the slow axis orientation approaches 0° (or 90° direction). Such phenomenon of grooves formation only in two directions is interpreted in terms of the surface energy in a MgO single crystal. According to the calculation by G. W. Watson *et al.*, the ratios of the surface energies are $E_{\{110\}}/E_{\{100\}} \approx 2.4$ and $E_{\{111\}}/E_{\{100\}} \approx 3.1$ [34]. This means that the {100} plane in a MgO single crystal is a slip plane with the lowest surface energy. Therefore, it is easier to increase the interfacial area in {100} plane than in other planes, leading to ease formation of defects and nanovoids along <100> and <010> directions. These structural changes are unique to crystals with a large difference between surface energies in slip plane and other planes. In the case of the crystal with smaller differences in surface energy, for example, LiF crystal, it is seemingly possible to form nanovoids in the direction along the {110} plane, which is not a slip plane (not shown here). For the ultraprecision machining of crystals by laser, understanding the origin of structural modification is key. Details should be needed to be addressed in future studies. We have also observed the detailed structure in the upper part of the processed region by TEM. The periodic bright regions with approximately 100 nm intervals in the [010] direction were observed in the bright field image [Fig. 3]. These regions were analyzed consist of oxygen defects and/or nanovoids.

On the other hand, in the lower part of the processed region, we observed cross-shaped grooves with about 1 μm width at the center part [Fig. 2(b, d, f)]. The direction of these grooves was parallel to the {100} plane and did not depend on the laser polarization direction. We have concluded that such grooves can be formed by laser filamentation. It is known that laser filamentation can be generated by the balance between self-focusing due to the optical Kerr effect and plasma defocusing. The threshold P_{Cr} for filamentation is expressed by the equation [35]:

$$P_{\mathrm{cr}} = \frac{\pi(0.61)^2{\lambda_0}^2}{8n_0n_2} \quad (1)$$

where λ_0 is the laser wavelength, n_0 is the refractive index, and n_2 is the nonlinear refractive index.

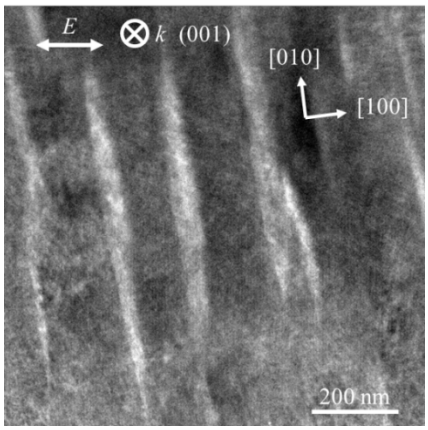

Fig. 3 The bright field TEM image of the upper part in the laser-processed region. Symbols of *E* and *k* show the laser polarization and propagation direction, respectively.

Using 800 nm, 1.72 and 1.61×10^{-19} m^2/W [36] respectively, P_{Cr} is calculated to be about 0.34 MW. From our experimental conditions, the laser peak power is also obtained to be about 0.20 GW, which greatly exceeds the threshold. Such high peak power causes multiple filamentations. Although multiple filamentations were presumed to occur randomly [37], it has been recently reported that multiple filaments regularly formed in water or in crystals [38,39]. For a MgO single crystal, multiple filaments with a symmetric pattern as shown in Fig. 6(a) may cause the cross-shaped grooves. Furthermore, the cross-shaped grooves are mainly composed of rhombic dots with vertices in the [100] and [010] directions. Such structure may be the cause of a spot without birefringence observed in Fig.1 (b).

4. Laser writing of traces

We have performed direct laser writing of traces with scanning in the [100] or [010] direction [Fig. 4]. In the case that the laser polarization direction is nearly perpendicular to the scanning direction (0° ~ 30° or 45° ~ 90° for the scanning direction of [010] or [100], respectively), the polarization-dependent birefringence with the slow axis perpendicular to the laser polarization was observed. This has a similar birefringence behavior to that for the fixed-point irradiation experiments. In the case of a nearly parallel between the laser polarization direction and the scanning direction, we observed different birefringence between the inner and outer part of the processed region. In this case, the slow axis direction in the inner part was parallel to the polarization direction, while that in the outer part was perpendicular.

To clarify the cause of different birefringence between the inner and outer parts, we performed FE-SEM observation for the upper and lower parts of the processed region by changing the polishing depth in steps. The lower part was located at about 60 μm deeper than the upper part. The surface after polishing was also chemically etched. In the upper part of the processed region [Fig. 5(a)], grooves were observed only in the [100] and [010] directions, which are similar to the results in the fixed-point irradiation experiments [Fig. 2(a, c, e)]. On the other hand, in the lower part of the processed region [Fig. 5(b)], the grooves were formed along the [100] direction, corresponding to the scanning direction,

despite the laser polarization direction. For the scanning in [010] direction, the grooves along [010] direction in the lower part of the processed region were also observed (not shown here). Therefore, we can conclude that the grooves in the upper and lower part is derived from different structural changes. That in the upper part originates from nanostructures induced by laser irradiation perpendicular to the polarization direction. On the other hand, that in the lower part is due to optical breakdown and formed parallel to the scanning direction. These different structures show different birefringence. For the measurement of retardation in birefringence, we used a transmission polarization microscope.

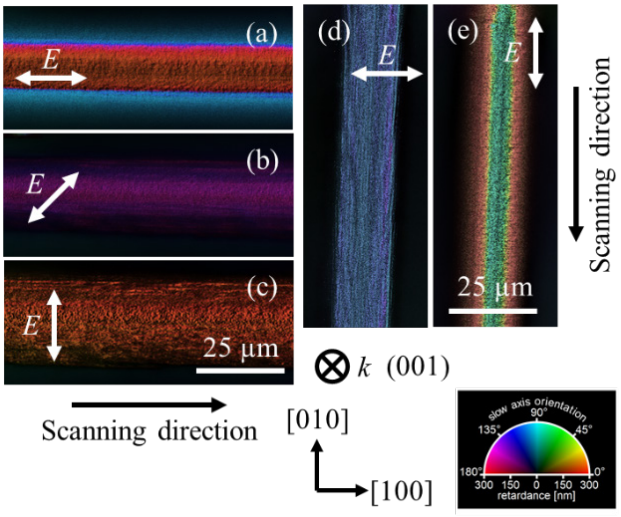

Fig. 4 The polarized optical microscope images of the laser-processed region in MgO (001) plane. The laser scanning direction was (a-c) [100] or (d, e) [010]. The laser polarization direction (E) was changed. Symbol k shows the laser propagation direction along [001].

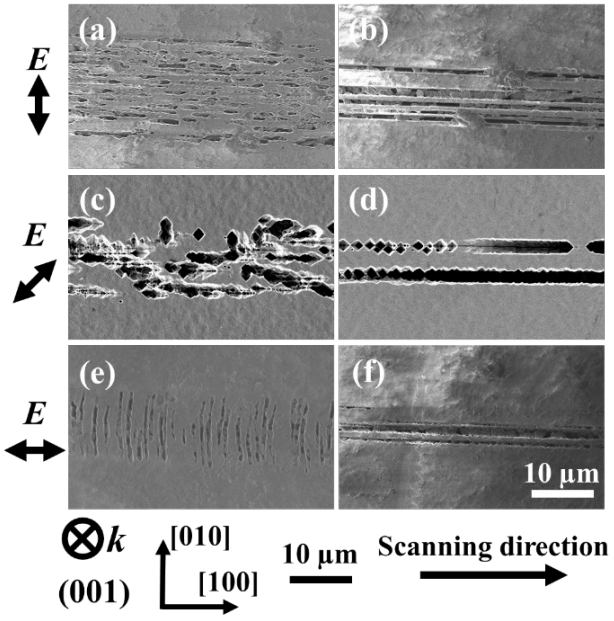

Fig. 5 The SEIs in the upper (a, c, e) and lower (b, d, f) parts of the laser-processed region. The laser parameters are 800 nm, 1 kHz, 100 fs, 20 μJ, and 100 μm/s, respectively.

In general, the retardation (Γ) is determined from the equation:

$$\Gamma = \frac{2\pi(n_e - n_0)t}{\lambda} \quad (2)$$

where n_e and n_o are the extraordinary and ordinary refractive indices, respectively, t is the thickness of the photoinduced birefringent region and λ is the wavelength (= 546 nm). Since we observed the laser-processed region by using a transmission polarization microscope, the total information of birefringence through the processed region was integrated. According to the azimuth of the transmission polarization microscope image, the nanostructures in the upper part mainly affected the birefringence in the inner part, while the structure in the lower part affected that in the outer part. We have interpreted the formation mechanism of grooves along the scanning direction as follows: The multiple filaments with a certain symmetric pattern are generated in the lower part of the focus region. Such multiple filaments cause the rhombic damaged regions with vertices in the [100] and [010] directions [Fig. 6(a)]. These damaged regions are continuously formed during the scanning and develop into grooves. Finally, the grooves were aligned along the scanning direction regardless of the polarization direction [Fig. 6(b)].

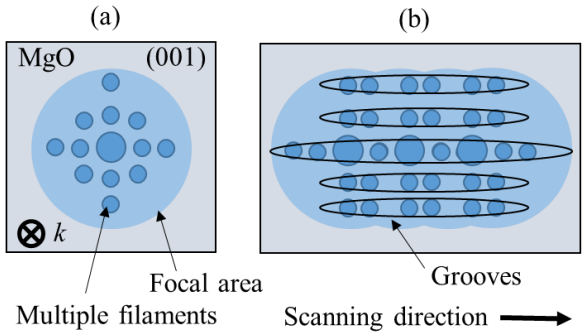

Fig. 6 The proposed model for the laser damage in the lower part of the laser-processed region based on the multiple filaments in the case of (a) fixed-point irradiation and (b) laser scanning.

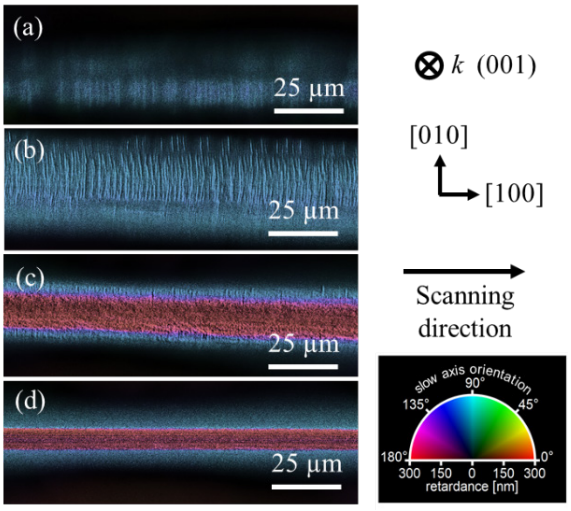

Fig. 7 The polarized optical microscope images of the laser-processed region by the objective lens with different NA of (a) 0.30, (b) 0.45, (c) 0.80, and (d) 0.90, respectively.

To confirm the contribution of multiple filamentations, we tuned the energy influences at the focus by changing the objective lens with different NAs (0.30, 0.45, 0.80, and 0.90). The femtosecond laser pulses with the same pulse energy of 20 μJ were focused inside a MgO sample through the four different objective lenses [Fig. 7]. Fig. 7 clearly shows that the slow axis orientation of the birefringence in the inner and outer part of the processed region is different in the case of the higher energy fluences. On the other hand, no apparent birefringence with the slow axis orientation parallel to the scanning direction was observed for the lower energy fluences, namely, only the polarization-dependent birefringence was observed. This means the grooves in the lower part are formed only in higher energy fluences. These results support our proposed model.

5. Summary

The birefringence with a slow axis orientation perpendicular to the laser polarization can be successfully photoinduced inside a MgO single crystal. Such birefringence is caused by the distribution of oxygen defects and nanovoids in the direction along the {100} slip plane. In the case of the laser irradiation to MgO (001) plane, the existence ratio of defects and nanovoids in [100] or [010] direction was changed according to the laser polarization direction. In addition, depending on the laser energy, the damage traces along the scanning direction were also observed in the lower part of the processed region due to multiple filamentations.

References

[1] F. Flamini, L. Magrini, A. S. Rab, N. Spagnolo, V. D. Ambrosio, P. Mataloni, F. Sciarrino, T Zandrini, A. Crespi, R. Ramponi, and R. Osellame: Light Sci. Appl., 4, (2015) e354.

[2] M. Li, J. Ling, Y. He, U. A. Javid, S. Xue, and Q. Lin: Nat. Commun., 11, (2020) 4123.

[3] A. H. A. Lutey, L. Gemini, L. Romoli, G. Lazzini, F. Fuso, M. Faucon, and R. Kling: Sci. Rep., 8, (2018) 10112.

[4] I. Conrad-Hengerer, M. A. Sheikh, F. H. Hengerer, T. Schultz, and H. B. Dick: J. Cataract Refract. Surg., 41, (2015) 1356.

[5] A. Lacraz, M. Polis, A. Theodosiou, C. Koutsides, and K. Kalli: IEEE Photon. Technol. Lett., 27, (2015) 693.

[6] S. Bai, D. Serien, A. Hu, and K. Sugioka: Adv. Funct. Mater., 28, (2018) 1706262.

[7] K. M. Davis, K. Miura, N. Sugimoto, and K. Hirao: Opt. Lett., 21, (1996) 1729.

[8] K. Miura, J. Qui, H. Inouye, T. Mitsuyu, and K. Hirao: Appl. Phys. Lett., 71, (1997) 3329.

[9] A. Dragomir, D. N. Nikogosyan, K. A. Zagorulko, P. G. Kryukov, and E. M. Dianov: Opt. Lett., (2003) 2171.

[10] S. J. Mihailov, C. W. Smelser, P. Lu, R. B. Walker, D. Grobnic, H. Ding, G. Henderson, and J. Unruh: Opt. Lett., 28, (2003) 995.

[11] E. N. Glezer, M. Milosavljevic, L. Huang, R. J. Finlay, T.-H. Her, J. P. Callan, and E. Mazur: Opt. Lett., 21, (1996) 2023.

[12] Y. Shimotsuma, M. Sakakura, P. G. Kazansky, M. Beresna, J. Qiu, K. Miura, and K. Hirao: Adv. Mater., 22, (2010) 4039.

[13] M. Gertsvolf, H. Jean-Ruel, P. P. Rajeev, D. D. Klug, D. M. Rayner, and P. B. Corkum: Phys. Rev. Lett., 101, (2008) 243001.

[14] S. Kanehira, K. Miura, K. Fujita, K. Hirao, J. Si, N. Shibata, and Y. Ikuhara: Appl. Phys. Lett., 90, (2007) 163110.

[15] C. Moon, S. Kanehira, M. Nishi, K. Miura, T. Nakaya, E. Tochigi, N. Shibata, Y. Ikuhara, and K. Hirao: J. Am. Ceram. Soc., 92, (2009) 3118.

[16] M. Sakakura, T. Tochio, M. Eida, Y. Shimotsuma, S. Kanehira, M. Nishi, K. Miura, and K. Hirao: Opt. Express, 19, (2011) 17780.

[17] T. Tochio, M. Sakakura, Y. Shimotsuma, M. Nishi, K. Hirao, and K. Miura: Jpn. J. Appl. Phys., 51, (2012) 126602.

[18] M. Sakakura, Y. Shimotsuma, N. Fukuda, and K. Miura: J. Appl. Phys., 118, (2015) 023106.

[19] Y. Shimotsuma, K. Kinouchi, R. Yanoshita, M. Fujiwara, N. Mizuochi, M. Uemoto, M. Shimizu, and K. Miura: Opt. Express, 31, (2023) 1594.

[20] Y. Shimotsuma, P. G. Kazansky, J. Qiu, and K. Hirao: Phys. Rev. Lett., 91, (2003) 247405.

[21] Y. Shimotsuma, T. Asai, M. Sakakura, and K. Miura: J. Laser Micro Nanoeng., 9, (2014) 31.

[22] S. Mori, T. Kurita, Y. Shimotsuma, M. Sakakura, M. Kiyotaka: J. Laser Micro Nanoeng., 11, (2016) 87.

[23] T. Okada, T. Tomita, S. Matsuo, S. Hashimoto, Y. Ishida, S. Kiyama, and T. Takahashi: J. Appl. Phys., 106, (2009) 054307.

[24] M. Mori, Y. Shimotsuma, T. Sei, M. Sakakura, K. Miura, and H. Udono: Phys. Status Solidi A, 212, (2015) 715.

[25] Y. Toyama, Y. Shimotsuma, M. Shimizu, and K. Miura: Annual meeting of Laser Society of Japan, (2021) D07-20p-IV-05.

[26] Y. Nakanishi, Y. Shimotsuma, M. Sakakura, M. Shimizu, and K. Miura: Proc. SPIE, Vol. 10520, (2018) 105201J.

[27] Y. Shimotsuma, Y. Nakanishi, M. Shimizu, M. Sakakura, and K. Miura: Proc. SPIE, Vol. 10536, (2018) 105361U.

[28] J. E. Wertz, P. Auzins, R. A. Weeks, and R. H. Silsbee: Phys. Rev., 107, (1957) 1535.

[29] W. A. Sibley and Y. Chen: Phys. Rev., 160, (1967) 712.

[30] D. Wortmann, J. Gottmann, N. Brandt, and H. Horn-Solle: Opt. Express, 16, (2008) 1517.

[31] Y. Shimotsuma, K. Hirao, J. Qiu, and P. G. Kazansky: Mod. Phys. Lett., B 19, (2005) 225.

[32] F. Zhang, Z. Nie, H. Huang, L Ma, H. Tang, M. Hao, and J. Qiu: Opt. Express, 27, (2019) 6442.

[33] E. Simova, P.P. Rajeev, C. Hnatovsky, R.S. Taylor, D.M. Rayner, P.B. Corkum, and V.R. Bhardwaj: Phys. Rev. Lett., 96 (2006) 057404.

[34] G. W. Watson, E. T. Kelsey, N. H. de Leeuw, D. J. Harris, and S. C. Parker: J. Chem. SOC. Faraday Trans., 92, (1996) 433.

[35] R. W. Boyd: Nonlinear Optics (Academic Press, U.S, 2003) p.315.

[36] R. Adair, L. L. Chase, and S. A. Payne: Phys. Rev. B, 39, (1989) 3337.

[37] I. Bespalov and V. I. Talanov: JETP Lett., 3 (1966) 307.

[38] A. Dubietis, G. Tamošauskas, G. Fibich, and Boaz Ilan:
Opt. Lett., 29, (2004) 10.
[39] L. Bryukvina: J. Lumin., 162 (2015) 145.

(Received: July 10, 2023, Accepted: January 6, 2024)